Motion of Nanodroplets near Chemical Heterogeneities

A. Moosavi,* M. Rauscher,* and S. Dietrich*

Max-Planck-Institut für Metallforschung, Heisenbergstr. 3, D-70569 Stuttgart, Germany, and Institut für Theoretische und Angewandte Physik, Universität Stuttgart, Pfaffenwaldring 57, D-70569 Stuttgart, Germany

Received June 14, 2007. In Final Form: October 18, 2007

We investigate the dynamics of nanoscale droplets in the vicinity of chemical steps which separate parts of a substrate with different wettabilities. Due to long-ranged dispersion forces, nanodroplets positioned on one side of the step perceive the different character of the other side even at a finite distance from the step, leading to a dynamic response. The direction of the ensuing motion of such droplets depends not only on the difference between the equilibrium contact angles on these two parts but in particular on the difference between the corresponding Hamaker constants. Therefore, the motion is not necessarily directed toward the more wettable side and can also be different from that of droplets which span the step.

I. Introduction

The interest in dynamical wetting phenomena has increased significantly with the development of micro- and nanofluidic systems, which allow one to handle minute amounts of liquid containing, for example, DNA or proteins for chemical analysis and biotechnology.[1,2] In particular, chemically heterogeneous systems with tailored, spatially varying wetting properties have found important applications in this context.[3,4] In open microfluidic systems, fluids are transported on chemical channels, that is, lyophilic stripes embedded in lyophobic substrates. While present devices are based mostly on micrometer sized channels, further miniaturization down to the nanoscale is clearly on the road map. This will eventually lead to nanofluidic systems for which a variety of physical phenomena, which on the microscale and above are either irrelevant or summarized into boundary conditions, become important.[5,6] For the optimization of the performance of nanofluidic systems, it is critical to understand the basic fluidic issues occurring on those scales. Recent theoretical studies of nanoscale fluids on chemically[7] and topographically[8] structured substrates have underscored the importance of such investigations.

Those analytical tools[9−12] which rely on classical macroscopic theory are not adequate for this purpose. However, there is a variety of techniques which allow one to study the present issues numerically such as molecular dynamics simulations[7,13] or standard computational fluid dynamics routines.[8] To a large extent, the available numerical investigations are based on solving thin film equations.[14−18] In most of theses studies, the chemical heterogeneities are introduced via abrupt, lateral changes of those parameters which characterize the potentials of homogeneous substrates.[14,16,17] However, this does not capture the actual behavior of such substrate potentials, even if the underlying chemical steps are taken to be atomically sharp.[19] Smooth chemical heterogeneities have been studied in ref 18 by introducing a continuously varying Hamaker constant. However, this approach is only applicable for very smooth variations of the wetting properties. Studies of the dynamics of droplets in the vicinity of topographic steps have shown that on the nanoscale a detailed modeling of the substrate and thus of the resulting effective interface potential is mandatory.[8] For a chemical step, this has been worked out within the framework of microscopic density functional theory with a view on the morphology of static wetting films.[20−22]

Here, we study the paradigmatic case of the dynamics of a nanodroplet of a simple liquid in the vicinity of a chemical step, that is, near a sharp and straight boundary between two parts of a substrate with different wetting properties. Because we want to focus on the effect of chemical rather than topographical heterogeneities (in contrast to ref 8), we assume the substrate surface to be smooth and flat, although in many experimental systems chemical steps are accompanied by a small topographical step of a few angstroms up to a nanometer in height. We assume the step to be formed by two adjacent quarter spaces composed of different substrate particles, and we analyze the driving force on the droplets and perform numerical calculations assuming Stokes flow as the underlying dynamics.

For numerical reasons, we restrict our analysis to two-dimensional (2D) droplets, corresponding to three-dimensional (3D) liquid ridges (or rivulets) which are translationally invariant in the direction parallel to the step. Such liquid ridges have been experimentally studied, for example, in ref 23. While rivulets can be unstable with respect to pearling (i.e., the breakup into

* To whom correspondence should be addressed. E-mail: moosavi@mf.mpg.de (A.M.); rauscher@mf.mpg.de (M.R.); dietrich@mf.mpg.de (S.D.).

(1) Karniadakis, G.; Beskok, A.; Aluru, N. *Microflows and Nanoflows: Fundamentals and Simulation,* 2nd ed.; Springer: NewYork, 2005.
(2) Dietrich, S.; Popescu, M. N.; Rauscher, M. *J. Phys.: Condens. Matter* **2005**, *17*, S577.
(3) Chaudhury, M. K.; Whitesides, G. M. *Science* **1992**, *256*, 1539.
(4) Kusumaatmaja, H.; Yeomans, J. M. *Langmuir* **2007**, *23*, 956.
(5) Eijkel, J. C. T.; van den Berg, A. *Microfluid. Nanofluid.* **2005**, *1*, 249.
(6) Mukhopadhyay, R. *Anal. Chem.* **2006**, *78*, 7379.
(7) Cieplak, M.; Koplik, J.; Banavar, J. R. *Phys. Rev. Lett.* **2006**, *96*, 114502.
(8) Moosavi, A.; Rauscher, M.; Dietrich, S. *Phys. Rev. Lett.* **2006**, *97*, 236101.
(9) Greenspan, H. P. *J. Fluid Mech.* **1978**, *84*, 125.
(10) Raphaël, E. *C. R. Acad. Sci., Ser. II* **1988**, *306*, 751.
(11) Brochard, F. *Langmuir* **1989**, *5*, 432.
(12) Subramanian, R. S.; Moumen, N.; McLaughlin, J. B. *Langmuir* **2005**, *21*, 11844.
(13) Yaneva, J.; Milchev, A.; Binder, K. *J. Chem. Phys.* **2004**, *121*, 12632.
(14) Schwartz, L. W.; Eley, R. R. *J. Colloid Interface Sci.* **1998**, *202*, 173.
(15) Brusch, L.; Kühne, H.; Thiele, U.; Bär, M. *Phys. Rev. E* **2002**, *66*, 011602.
(16) Pismen, L. M.; Thiele, U. *Phys. Fluids* **2006**, *18*, 042104.
(17) Zhao, Y.; Marshall, J. S. *J. Fluid Mech.* **2006**, *559*, 355.
(18) Thiele, U.; Knobloch, E. *New J. Phys.* **2006**, *8*, 313.
(19) Koch, W.; Dietrich, S.; Napiórkowski, M. *Phys. Rev. E* **1995**, *51*, 3300.
(20) Bauer, C.; Dietrich, S. *Phys. Rev. E* **1999**, *60*, 6919.
(21) Bauer, C.; Dietrich, S. *Eur. Phys. J. B* **1999**, *10*, 767.
(22) Bauer, C.; Dietrich, S. *Phys. Rev. E* **2000**, *61*, 1664.
(23) Ondarçuhu, T.; Veyssié, M. *J. Phys. II* **1991**, *1*, 75.

10.1021/la7017677 CCC: $40.75
Published on Web 01/08/2008

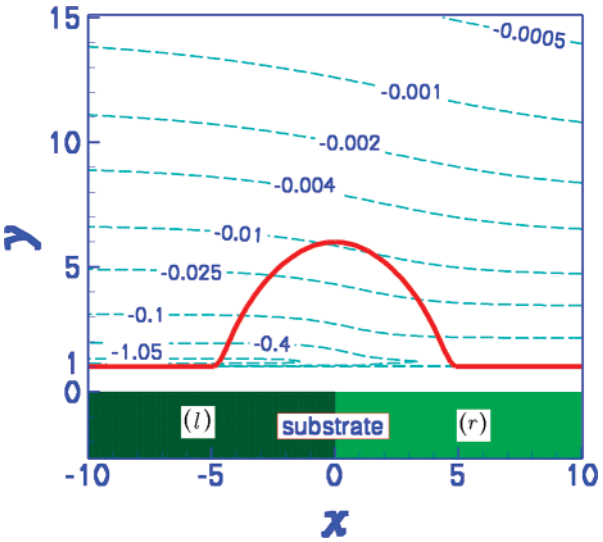

Figure 1. The chemical step is translationally invariant along the *z*-axis (orthogonal to the image plane). A nanodroplet (full line) is exposed to the vertically and laterally varying disjoining pressure, the contour plot of which is shown. Here, both sides of the substrate are chosen to correspond to the Θ case with $\theta_{eq}^{(l)} = 97.2°$ ($B^{(l)} = 0$, $C^{(l)} = 3$) and $\theta_{eq}^{(r)} = 51.3°$ ($B^{(r)} = 0$, $C^{(r)} = 1$, $q = 1$) (see eqs 8 and 9). Lengths and the disjoining pressures are measured in units of $b^{(l)}$ and $\sigma/b^{(l)}$, respectively. A coating of the substrate is not indicated, as here $B^{(l)} = B^{(r)} = 0$, so that for $x \to \pm\infty$ the equilibrium thicknesses of the underlying wetting film are the same, that is, $y_0^{(l)} = y_0^{(r)} = y_0 = b^{(l)}$.

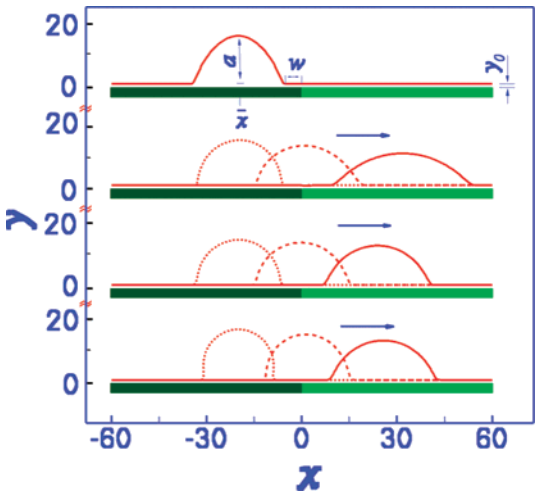

Figure 2. Motion of a nanodroplet across three different chemical steps for the Θ case on both sides and for $B^{(l)} = 0$, $B^{(r)} = 0$, and $q = b^{(r)}/b^{(l)} = 1.0$ so that $y_0^{(l)} = y_0^{(r)}$. The uppermost part shows the initial interface profile. The parameters for the lower three parts are $\theta_{eq}^{(l)} = 97.2°$ ($C^{(l)} = 3$), $\theta_{eq}^{(r)} = 51.3°$ ($C^{(r)} = 1$); $\theta_{eq}^{(l)} = 97.2°$ ($C^{(l)} = 3$), $\theta_{eq}^{(r)} = 75.5°$ ($C^{(r)} = 2$); and $\theta_{eq}^{(l)} = 120°$ ($C^{(l)} = 4$), $\theta_{eq}^{(r)} = 75.5°$ ($C^{(r)} = 2$) from top to bottom. This means that in all three cases the right part of the substrate is the more wettable one. The profiles correspond to times $t = 355$, 2000, and 22 025; $t = 375$, 8125, and 24 300; and $t = 185$, 7800, and 23 500, respectively, in units of $\mu b^{(l)}/(C^{(l)}\sigma)$.

droplets; see ref 24) and therefore might be not particularly relevant for practical applications, we expect that our results will carry over qualitatively to the behavior of 3D droplets. Unless the drop touches or spans the chemical step, the force on the droplet (defined in, cf., eq 16) is expected to have the same sign in two and three spatial dimensions.

Since the direction of motion of the droplets is determined by the forces acting on the droplet, it will be independent of the underlying dynamics. However, the absolute value of the velocity depends on the dynamics. Comparisons with molecular dynamics simulations have shown that hydrodynamic equations reliably describe the flow of minute amounts of simple liquids on spatial scales down to a few molecular diameters close to confining walls.[25,26] Below these scales, the structure of the liquid deviates from the bulk structure in that molecular layering can occur. The droplets reside on and are connected to wetting films with thicknesses on such microscopic scales (see Figure 1 and ref 27). Therefore, the dynamics in these wetting films is not well described by the Stokes dynamics we use. However, these wetting films exhibit little internal dynamics, as they are thin and strongly coupled to the substrate. Within our approach, the influence of these wetting films on the droplet dynamics is limited to removing the stress singularity at the moving three-phase contact line. It has turned out that on this basis a quantitatively reliable *hydrodynamic* modeling of the dewetting dynamics of (even only a few nanometers thick) polymer films is possible.[28] The paper is organized such that in the following section II we discuss the disjoining pressure in the vicinity of a chemical step, and in section III we discuss the mesoscopic hydrodynamics of the droplets. In section IV, we relate the droplet dynamics to the disjoining pressure induced forces and we discuss, inter alia, the relevance of our findings for experimental systems in section V. In section VI, we summarize our results and provide our conclusions.

II. Modeling of Chemical Heterogeneities

As depicted in Figure 1, we consider a partially wetting, nonvolatile, and incompressible liquid forming a nanodroplet on top of a wetting film over a chemical step. The type of chemical step which we consider here can be viewed as being composed of two different quarter spaces with each of the two corresponding upper surfaces coated additionally with a thin layer of a different material. Assuming purely additive intermolecular interactions, we can decompose the disjoining pressure into its contributions from four building blocks, that is, the two quarter spaces forming the substrate and the two coating layers on the respective parts.

A. The Edge as a Building Block. First, we consider an edge without surface coating, say the left part of the substrate shown in Figure 1, which we denote by the superscript (l). Assuming Lennard−Jones type intermolecular pair potentials $V_{\alpha\beta}(r) = M_{\alpha\beta}/r^{12} - N_{\alpha\beta}/r^6$, where $M_{\alpha\beta}$ and $N_{\alpha\beta}$ are material parameters and α and β relating to the liquid inside the droplet and precursor film (l), the surrounding vapor or gas (l′), the substrate (s), or the coating (c), the local disjoining pressure (DJP) corresponding to an edge occupying $\Omega_s^{(l)} = \{\mathbf{r} \in \mathrm{R}^3 | x \le 0, y \le 0, z \in \mathrm{R}\}$ is given by[21,29]

$$\Pi_e^{(l)}(x,y) = \int_{\Omega_s^{(l)}} \frac{\Delta M^{(l)}}{|\mathbf{r}-\mathbf{r}'|^{12}} d^3r' - \int_{\Omega_s^{(l)}} \frac{\Delta N^{(l)}}{|\mathbf{r}-\mathbf{r}'|^6} d^3r' = \Delta M^{(l)} I_e^{12(l)}(x,y) - \Delta N^{(l)} I_e^{6(l)}(x,y) \quad (1)$$

with $\Delta M^{(l)} = \rho_l^2 M_{ll} + \rho_{l'}\rho_s^{(l)} M_{sl'}^{(l)} - \rho_l\rho_{l'} M_{ll'} - \rho_l\rho_s^{(l)} M_{sl}^{(l)}$ and $\Delta N^{(l)}$

(24) Brinkmann, M.; Kierfeld, J.; Lipowsky, R. *J. Phys.: Condens. Matter* **2005**, *17*, 2349.
(25) Thompson, P. A.; Robbin, M. O. *Phys. Rev. A* **1990**, *41*, 6830.
(26) Koplik, J.; Lo, T. S.; Rauscher, M.; Dietrich, S. *Phys. Fluids* **2006**, *18*, 032104.
(27) Dietrich, S. In *Phase Transitions and Critical Phenomena*; Domb, C., Lebowitz, J. L., Eds.; Academic: London, 1988; p 1.
(28) Becker, J.; Grün, G.; Seemann, R.; Mantz, H.; Jacobs, K.; Mecke, K. R.; Blossey, R. *Nat. Mater.* **2003**, *2*, 59.

$= \rho_l^2 N_{ll} + \rho_{l'}\rho_s^{(l)} N_{sl'}^{(l)} - \rho_l\rho_{l'} N_{ll'} - \rho_l\rho_s^{(l)} N_{sl}^{(l)}$, where ρ_l, $\rho_{l'}$, and $\rho_s^{(l)}$ are the number densities of the liquid, the surrounding fluid, and the substrate, respectively. In many systems, the density of the surrounding gas or vapor is negligible, and in the case that it is the vapor-phase corresponding to the liquid, one has $M_{ll} = M_{ll'}$ and $N_{ll} = N_{ll'}$. Equation 1 is also valid for two-fluid systems with a second immiscible liquid instead of the gas or vapor; however, the dynamics of such a system differs significantly from the model in section III. The edge geometry allows one to analytically calculate both integrals in eq 1, that is, $I_e^{12(l)}$ and $I_e^{6(l)}$, respectively. As we shall show below, $\Delta N^{(l)}$ is proportional to the Hamaker constant of a semi-infinite substrate composed of that material which forms the left part of the substrate.

B. The Contribution of a Thin Coating Layer. The contribution of a thin coating layer of thickness $d^{(l)}$ on the upper part of an edge $\Omega_c^{u(l)} = \{\mathbf{r} \in R^3 | x \le 0, -d^{(l)} \le y \le 0, z \in R\}$ to the disjoining pressure is

$$\Delta N'^{(l)} I_c^{u(l)}(x, y) = -\int_{\Omega_c^{u(l)}} \frac{\Delta N'^{(l)}}{|\mathbf{r} - \mathbf{r}'|^6} d^3r' \qquad (2)$$

with $\Delta N'^{(l)} = \rho_l^2 N_{ll} - \rho_l\rho_c^{(l)} N_{cl}^{(l)}$. Here, we have neglected the effect of the repulsive part of the liquid-coating interaction which gives rise to a contribution shorter ranged ($\sim y^{-10}$) than the corresponding term ($\sim y^{-9}$) arising in $I_e^{12(l)}(x, y)$.[20,30] The DJP of an edge including the coating of its upper side is therefore given by

$$\Pi_{ce}^{(l)}(x, y) = \Pi_e^{(l)}(x, y + d^{(l)}) + \Delta N'^{(l)} I_c^{u(l)}(x, y) \qquad (3)$$

C. Building the Chemical Step. The DJP contribution from the right-hand side of the substrate (marked with a superscript (r)) can be obtained analogously. Since the corresponding integrals $I_e^{12(r)}$, $I_e^{6(r)}$, and $I_c^{u(r)}$ for the right-hand side are the mirror images (with respect to the yz-plane) of their counterparts for the left-hand side, the former ones can be expressed in terms of the latter ones, leading to

$$\Pi_{ce}^{(r)}(x, y) = \Delta M^{(r)} I_e^{12(l)}(-x, y + d^{(r)}) - \Delta N^{(r)} I_e^{6(l)}(-x, y + d^{(r)}) + \Delta N'^{(r)} I_c^{u(l)}(-x, y) \qquad (4)$$

We shall only consider coatings which are thin compared with the wetting film. For $x \to \pm\infty$, the DJP of the coated edge reduces to that of a coated, laterally homogeneous substrate:

$$\Pi_{ch}^{(r)}(y) = \frac{\pi\Delta M^{(r)}}{45y^9} - \frac{\pi\Delta N^{(r)}}{6y^3} + \frac{\pi\Delta N''^{(l)} d^{(r)}}{2y^4} \qquad (5a)$$

$$\Pi_{ch}^{(l)}(y) = \frac{\pi\Delta M^{(l)}}{45y^9} - \frac{\pi\Delta N^{(l)}}{6y^3} + \frac{\pi\Delta N''^{(l)} d^{(l)}}{2y^4} \qquad (5b)$$

with $\Delta N''^{(r)} = \Delta N^{(r)} - \Delta N'^{(r)}$ and $\Delta N''^{(l)} = \Delta N^{(l)} - \Delta N'^{(l)}$. The equilibrium thicknesses $y_0^{(l)}$ and $y_0^{(r)}$ of the wetting films on such substrates is given by the smallest positive zero of the DJP, that is, $\Pi_{ch}^{(l)}(y = y_0^{(l)}) = \Pi_{ch}^{(r)}(y = y_0^{(r)}) = 0$. The effective interface potentials corresponding to $\Pi_{ch}^{(r)}(y)$ and $\Pi_{ch}^{(l)}(y)$ are[30,31]

$$\Phi_{ch}^{(r)}(y) = \frac{\pi\Delta M^{(r)}}{360y^8} - \frac{\pi\Delta N^{(r)}}{12y^2} + \frac{\pi\Delta N''^{(r)} d^{(r)}}{6y^3} \qquad (6a)$$

$$\Phi_{ch}^{(l)}(y) = \frac{\pi\Delta M^{(l)}}{360y^8} - \frac{\pi\Delta N^{(l)}}{12y^2} + \frac{\pi\Delta N''^{(l)} d^{(l)}}{6y^3} \qquad (6b)$$

respectively. The second terms are usually written as $-H^{(r)}/(12\pi y^2)$ and $-H^{(l)}/(12\pi y^2)$, respectively, where $H^{(r)} = \pi^2\Delta N^{(r)}$ and $H^{(l)} = \pi^2\Delta N^{(l)}$ are the Hamaker constants of the right and left part of the substrate, respectively.

At this point, we introduce dimensionless quantities (marked by a asterisk) based on the coefficients of the DJP on the left part of the substrate. We measure lengths in units of $b^{(l)} = [2\Delta M^{(l)}/(15|\Delta N^{(l)}|)]^{1/6}$, which for $\Delta N^{(l)} > 0$ is the equilibrium wetting film thickness on the *uncoated* homogeneous substrate. For polymer films, this length scale is of the order of the radius of gyration R_g, typically of the order of 1 nm.[28] The pressure scale is given by the surface tension $\sigma/b^{(l)}$. With this, far from the edge ($x \to \pm\infty$), one has

$$\Pi_{ch}^{*(r)}(y_*) = C^{(r)}\left(\frac{q^9}{{y_*}^9} \pm \frac{q^3}{{y_*}^3} + \frac{q^4 B^{(r)}}{{y_*}^4}\right) \qquad (7a)$$

$$\Pi_{ch}^{*(l)}(y_*) = C^{(l)}\left(\frac{1}{{y_*}^9} \pm \frac{1}{{y_*}^3} + \frac{B^{(l)}}{{y_*}^4}\right) \qquad (7b)$$

with $q = b^{(r)}/b^{(l)}$, which is the ratio of the characteristic length scales on the two substrates ($b^{(r)} = [2\Delta M^{(r)}/(15|\Delta N^{(r)}|)]^{1/6}$). To avoid a clumsy notation in the following we drop the asterisks.

In eq 7, $B^{(r)} = \pi\Delta N''^{(r)} d^{(r)}/(2A^{(r)}b^{(r)4})$ and $B^{(l)} = \pi\Delta N''^{(l)} d^{(l)}/(2A^{(l)}b^{(l)4})$ quantify the strength of the coating, and $C^{(r)} = A^{(r)}b^{(l)}/\sigma$ and $C^{(l)} = A^{(l)}b^{(l)}/\sigma$ determine the strength of the disjoining pressures relative to the surface tension, where $A^{(r)} = \pi(\Delta M^{(r)}/45)^{-1/2}(|\Delta N^{(r)}|/6)^{3/2}$ and $A^{(l)} = \pi(\Delta M^{(l)}/45)^{-1/2}(|\Delta N^{(r)}|/6)^{3/2}$. We note that since the pressure scale is given in terms of $b^{(l)}$, it is also entering into the definition of $C^{(r)}$. Since a more refined analysis of the DJP beyond eq 1 yields $B^{(r)} \neq 0$ and $B^{(l)} \neq 0$ even in the absence of a coating layer,[27,30] in the following we consider $B^{(l)}$ and $B^{(r)}$ as independent parameters.

The contact angles $0 < \theta_{eq}^{(r)} < \pi$ and $0 < \theta_{eq}^{(l)} < \pi$ of macroscopic droplets on the right and left part of the substrate, repsectively, and those values of $C^{(r)}$, $C^{(l)}$, $B^{(r)}$, $B^{(l)}$, and q, which give rise to partial wetting, are related via

$$\cos\theta_{eq}^{(r)} = 1 + \int_{y_0^{(r)}}^{\infty} \Pi_{ch}^{(r)}(y)\, dy = 1 + \Phi_{ch}^{(r)}(y_0^{(r)}) \qquad (8a)$$

$$\cos\theta_{eq}^{(l)} = 1 + \int_{y_0^{(l)}}^{\infty} \Pi_{ch}^{(l)}(y)\, dy = 1 + \Phi_{ch}^{(l)}(y_0^{(l)}) \qquad (8b)$$

(see the insets of Figure 2 in ref 8). The actual contact angle of nanodroplets defined, for example, as their slope at the point of inflection or via a spherical extrapolation of their top cap toward the substrate, may differ from the macroscopic value depending on the size of the nanodroplets and details of the DJP.

In the second terms on the right-hand side of eq 7, the upper plus (lower minus) sign corresponds to $\Delta N^{(r)} < 0$ ($\Delta N^{(r)} > 0$) and $\Delta N^{(l)} < 0$ ($\Delta N^{(l)} > 0$), respectively. In the following, we shall refer to these cases as the plus $\oplus$ and the minus $\ominus$ cases. The dimensionless form of the DJP (in units of $\sigma/b^{(l)}$) for a single edge coated with a thin layer on the upper side is given by

(29) Robbins, M. O.; Andelman, D.; Joanny, J. F. *Phys. Rev. A* **1991**, *43*, 4344.
(30) Dietrich, S.; Napiórkowski, M. *Phys. Rev. A* **1991**, *43*, 1861.
(31) Napiórkowski, M.; Koch, W.; Dietrich, S. *Phys. Rev. A* **1992**, *45*, 5760.

$$\Pi_{ce}^{(r)}(x,y) = C^{(r)}\left[\frac{45q^9}{\pi} I_e^{12(l)}(-x,y) \pm \frac{6q^3}{\pi} I_e^{6(l)}(-x,y) - \frac{2q^4 B^{(r)}}{\pi} I_c^{u(l)}(-x,y)\right] \quad (9a)$$

$$\Pi_{ce}^{(l)}(x,y) = C^{(l)}\left[\frac{45}{\pi} I_e^{12(l)}(x,y) \pm \frac{6}{\pi} I_e^{6(l)}(x,y) - \frac{2B^{(l)}}{\pi} I_c^{u(l)}(x,y)\right] \quad (9b)$$

Due to the additivity of the interatomic potentials used here, the DJP of the chemical step can be obtained by superimposing the DJP of the constitutional parts, that is, the two edges coated on the upper side. Thus, the DJP of the whole substrate with a chemical step is given by

$$\Pi(x,y) = \Pi_{ce}^{(l)}(x,y) + \Pi_{ce}^{(r)}(x,y) \quad (10)$$

Figure 1 shows the contour lines of the DJP across a chemical step for a typical example.

III. Mesoscopic Hydrodynamics

To probe the influence of the DJP on droplets near and on chemical steps, we have performed mesoscopic hydrodynamic calculations based on the 2D Stokes equation for an incompressible liquid of viscosity μ on an impermeable substrate at which we impose a no-slip boundary condition, that is, $\mathbf{u} = 0$ at the substrate surface. While the disjoining pressure calculated in the previous section takes into account a gas or vapor phase or even a second fluid on top of the liquid, for the dynamics we assume the fluid to be surrounded by vacuum, that is, an inviscid and massless medium. Therefore, we solve the incompressible Stokes equation

$$\nabla\cdot\mathbf{u} = 0 \qquad \text{and} \qquad \mu\nabla^2\mathbf{u} = \nabla p \quad (11)$$

for the flow velocity $\mathbf{u} = (u_x, u_u)$ and the pressure p only within the liquid and set the tangential stresses at the liquid surface to zero. The normal stresses are balanced by the hydrostatic pressure, the surface tension, and the disjoining pressure, leading to[32,33]

$$\mathbf{n}\cdot\tau\cdot\mathbf{n} = -p + \sigma\kappa - \Pi \quad (12)$$

with the local mean curvature κ, the stress tensor τ, and the surface normal vector $\mathbf{n}$ pointing out of the liquid. By mass conservation of the nonvolatile liquid, the local normal velocity v of the liquid surface is given by $v = \mathbf{n}\cdot\mathbf{u}$ at the surface.

The equations of motion are cast into a dimensionless form by using the length scale $b^{(l)}$ and the pressure scale $\sigma/b^{(l)}$ introduced in the previous section together with the velocity scale $C^{(l)}\sigma/\mu$. The corresponding time scale is $\mu b^{(l)}/(\sigma C^{(l)})$. This means that, in the regime of low Reynolds numbers, for which the Stokes equation applies, the viscosity only sets the time scale of the dynamics but does not change the behavior of the droplets qualitatively.

We have solved theses equations numerically with a standard biharmonic boundary integral method.[32] This method is based on formulating the Stokes equation in terms of the stream function ψ, with $\partial_y\psi = u_x$ and $\partial_x\psi = -u_y$, and the vorticity $\omega = \partial_y u_x - \partial_x u_y$ so that eq 11 reads[32,33]

$$\nabla^2\psi = \omega \qquad \text{and} \qquad \nabla^2\omega = 0 \quad (13)$$

By invoking Green's second identity and the Rayleigh−Green identity, the above equations and therefore the whole dynamics is mapped onto that of the surface of the liquid. The boundary conditions can be written in terms of ψ and ω as well. At each time step, spatial discretization leads to a system of algebraic equations from which the local surface velocity can be calculated. The surface dynamics is integrated using an Euler scheme.[32,33]

As initial condition, for this overdamped dynamics, only the droplet shape has to be specified. To start reasonably close to the relaxed droplet shape, we choose a hemisphere centerd about $x = \bar{x}$ which is smoothly connected to the wetting layer, that is,

$$y(x; t = 0) = y_0 + a[1 - (|x - \bar{x}|/a)^2]^{|x-x|^m+1} \quad (14)$$

with the droplet height a in the center being equal to half the base width. The distance w of the droplet from the step is then given by $w = |\bar{x}| - a$ (see Figure 2). For $\bar{x} > 0$, the thickness y_0 of the wetting film is given by $y_0^{(r)}$, while we have $y_0 = y_0^{(l)}$ for $\bar{x} < 0$. In this study, we choose m, which specifies the smoothness of the transition region from the drop to the wetting layer, to be 10.

IV. Dynamics of Droplets

A. Chemical Steps without Coating. We first consider the case without coating ($B^{(l)} = B^{(r)} = 0$, which implies that ΔN is negative on both sides, corresponding to the $\ominus$ case) and with the same wetting film thickness ($q = 1$). Numerical results for different values of $C^{(r)}$ and $C^{(l)}$ are shown in Figure 2. At time $t = 0$, droplets of height $a = 15$ have been positioned at a distance $w = 5$ (see Figure 2) from the chemical step on the less wettable substrate. $C^{(l)}$, which describes the ratio of the intermolecular forces for the left side of the substrate and the surface tension, was selected such that $\theta^{(l)}$ is close to the contact angle of the initial droplet prepared with 90° (i.e., $4 \geq C^{(l)} \geq 3$), and therefore, during the *initial* relaxation of the prepared droplet *shape*, the distance of the leading edge of the droplet to the chemical step does not change significantly. Larger values of $C^{(l)}$ lead to larger values of $\theta^{(l)}$ for which the distance of the leading edge from the step would increase. For smaller values of $C^{(l)}$ (i.e., for $\theta^{(l)} \ll 90°$), the distance of the leading edge from the step decreases during the initial relaxation process and eventually crosses the step such that the droplet spans the step. This is not the case in which we are interested here. $C^{(r)}$ was chosen to be smaller than $C^{(l)}$, so that the right side of the substrate was more wettable. In all cases shown in Figure 2, the droplets gradually move to the right, that is, toward the more wettable side, as expected intuitively, and continue their motion there. This indicates that the nanodroplets can perceive the presence of the other part of the substrate even if the leading contact line is at a finite distance from the chemical step. As a function of time, the wetting layer thickness changes slightly, which is expected due to the change of the Laplace pressure as the droplet flattens on the more wettable right side.

B. Disjoining Pressure Induced Forces. On a homogeneous substrate, the equilibrium contact angle can be calculated from the DJP (see eq 8). Applying this formula to inhomogeneous substrates, one can define a spatially varying "local contact angle" via

$$\cos\theta(x) = 1 + \int_{y_0(x)}^{\infty} \Pi(x,y)\,dy = 1 + \Phi(x, y_0(x)) \quad (15)$$

with $\Pi(x, y_0(x)) = 0$. For $\Pi(x, y)$ rapidly varying as a function

(32) Kelmanson, M. A. *J. Eng. Math.* **1983**, *17*, 329.
(33) Betelú, S.; Thomas, L.; Gratton, R.; Marino, B. *Int. J. Numer. Methods Fluids* **1997**, *25*, 1.

of x (e.g., in the close vicinity of a chemical step), $\theta(x)$ does not resemble an actual contact angle. However, for large droplets, $\partial_x \theta(x)$ is related to the lateral force per unit length (of the ridge in z-direction) acting on a droplet in the direction parallel to the substrate surface but normal to the chemical step and induced by the disjoining pressure, that is,

$$f = \frac{1}{\Delta z}\int_{\partial\Omega_d} \Pi(x, y)\, n_x \, dS \qquad (16)$$

where $\partial\Omega_d$ is the 3D surface of the droplet (i.e., of the ridge), Δz is its length in the direction parallel to the step, and n_x is the x-component of the outward surface normal **n**.

For a microscopic droplet, the force f (per unit length) is a nontrivial function of its size. Here, we focus on nanodroplets which are large enough ($a > 10$) such that $\int_{y_0(x)}^{a} \Pi(x, y)\, dy \approx \int_{y_0(x)}^{\infty} \Pi(x, y)\, dy$. For these droplets, the force f in eq 16 can be approximately expressed in terms of the "local contact angles" (see eq 15) θ_r and θ_l at the right and left contact line, respectively. Parametrizing the droplet surface by $y = h(x)$ and splitting the integral in eq 16 into two parts, one for the left half and one for the right half of the droplet, expressing the integration in terms of an integral with respect to y, and comparing the two resulting integrals with the definition in eq 15, one obtains

$$f \approx \cos(\theta_r) - \cos(\theta_l) \approx \cos\,\theta(\bar{x} + a) - \cos\,\theta(\bar{x} - a) \qquad (17)$$

with the position of the droplet center denoted as $\bar{x}$ (see Figure 2). For smoothly varying DJP (which is only the case if both contact lines are on the same side of the chemical step and for $w \gg 1$), one has $\Pi(\bar{x} + a, y) - \Pi(\bar{x} - a, y) \approx 2a\partial_x \Pi(\bar{x}, y)$, so that for approximately symmetric droplets

$$f \approx -2a \sin\,\theta\; \partial\theta/\partial x|_{x=\bar{x}} \qquad (18)$$

If $\Pi(x, y)$ varies monotonically, f and $-\partial\theta/\partial x$ have the same sign even for larger droplets, that is, for droplets for which the difference of the cosines of the contact angles θ_r and θ_l cannot be expressed in terms of the gradient of $\theta(x)$. Since in the cases studied here the differences of the equilibrium contact angles on the two parts of the substrate are relatively small, we have estimated $f(\bar{x})$ by considering droplets with the shape used as the initial condition for the Stokes dynamics (see eq 14) but centered at $x = \bar{x}$.

Figure 3a shows $\theta(x)$ as defined in eq 15 in the vicinity of the chemical step for the parameters used in Figure 2. $\theta(x)$ monotonically decreases from $\theta_{eq}^{(l)}$ to $\theta_{eq}^{(r)}$ and, as shown in Figure 3b, the force acting on droplets of initial height $a = 15$ is positive for all positions $\bar{x}$ of the drop. The force curve has a rather flat, plateaulike shape with a maximum at $\bar{x} = 0$ and varies sharply if one of the contact lines is located near the chemical step. This result is in agreement with the numerical calculations, and it explains why the droplet speed decreases with the distance from the step.

C. Different Wetting Layer Thicknesses across the Step. In the case discussed in section 4.1, that is, with the same thicknesses of the wetting layer and without coating ($B^{(l)} = B^{(r)} = 0$ and $q = 1$), the local contact angle $\theta(x)$ changes monotonically from left to right (Figure 3a). This is not necessarily the case, in particular, for steps between materials generating different thicknesses of the wetting layer, and for two substrates with different forms of the DJP, that is, $\ominus$ on the left and $\oplus$ on the right side.

Figure 4 shows a contour plot of the DJP for a case in which the wetting layer thickness differs; here, $B^{(l)} = B^{(r)} = 0$ and $q = 1.25$ so that the wetting layer is thicker on the right side than on the left side. For this case, $\theta(x)$ and $f(\bar{x})$ are depicted in Figure 5; eq 8 reduces to $\cos\,\theta_{eq}^{(r)} = 1 - 0.375C^{(r)}q$ and $\cos\,\theta_{eq}^{(l)} = 1 - 0.375C^{(l)}$. With our choice for $C^{(l)} = 3$, one has $\theta_{eq}^{(r)} > \theta_{eq}^{(l)}$ for $C^{(r)} > 2.4$. However, outside a small region around the step, $\partial_x\theta > 0$ on both sides of the step for values of $C^{(r)}$ down to approximately 1.6. This means that for $1.6 < C^{(r)} < 2.4$ droplets are expected to move to the left even although the right part of the substrate has a smaller equilibrium contact angle. This is confirmed by analyzing the DJP induced force on the droplets (see Figure 5b). As in Figure 3, the force has a plateau for $\bar{x} \approx 0$, and for large droplets the plateau height is described well by eq 17. This figure also shows that drops spanning the step will move to the right for $1.6 < C^{(r)} < 2.4$ such that these drops as well as drops starting on the right-hand side will stop and get stuck with the left contact line pinned to the step. The reason for this is that f changes sign as this contact line crosses the chemical step. For $C^{(r)} > 2.4$, we observe a double sign change which indicates that a droplet starting on the now less wettable right-hand side will be stopped and pinned by the chemical step as it moves toward the left-hand side. This is also reflected in the

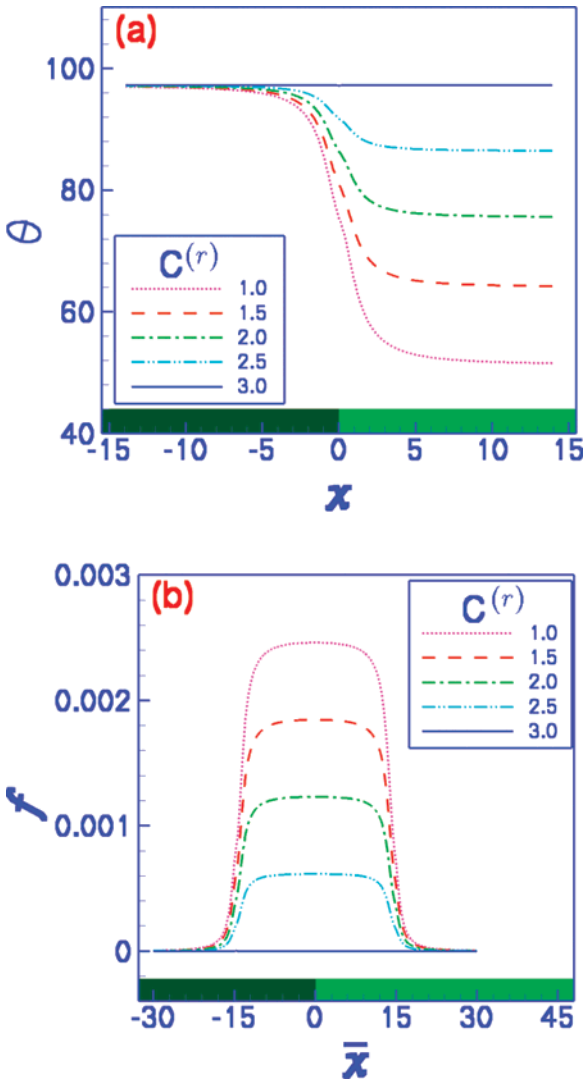

Figure 3. (a) "Local contact angle" $\theta(x)$ (see eq 15) and (b) lateral force $f(\bar{x})$ per unit length of the liquid ridge (eq 16) for droplets with $a = 15$ as a function of the droplet center $\bar{x}$ (see Figure 2) in the vicinity of a chemical step separating two parts of the substrate with $C^{(l)} = 3$, $B^{(l)} = B^{(r)} = 0$, and $q = 1$, for various values of $C^{(r)}$. Both substrate sides correspond to the $\ominus$ case. f is measured in units of σ.

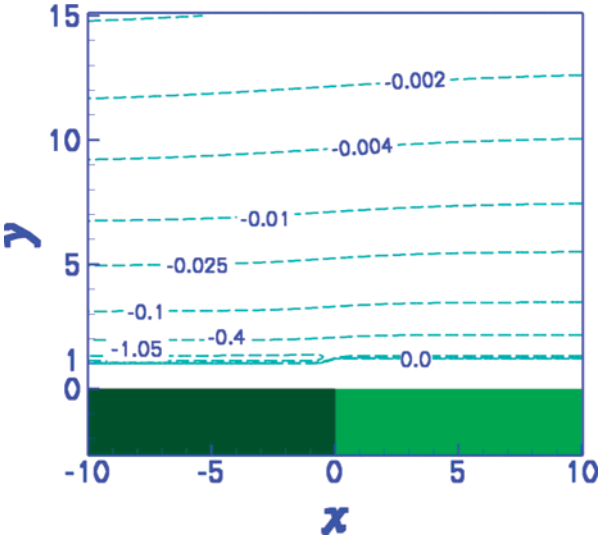

Figure 4. Contour plot of the DJP in the vicinity of a chemical step between two substrates with $C^{(l)} = 3$, $C^{(r)} = 2.15$, $B^{(l)} = B^{(r)} = 0$, and $q = 1.25$ (implying $\theta_{eq}^{(l)} = 97.2°$ and $\theta_{eq}^{(r)} = 90.4°$). Both parts of the substrate correspond to the $\ominus$ case.

change of $\theta(x)$ shown in Figure 5a, even though $\theta(x)$ loses its physical meaning close to $x = 0$.

To confirm these theoretical predictions, we have performed a series of numerical calculations by positioning a nanodroplet at a distance $w = 5$ on the right-hand side of the chemical step. For the case $C^{(r)} = 2.15$, that is, if the nanodroplet (with $a = 15$) is initially positioned on the more wettable part of the substrate, the results of these calculations are shown in Figure 6. This droplet moves to the left (i.e., counterintuitively toward the less wettable substrate), slows down, and stops when its advancing contact line touches the chemical step. A droplet initially spanning the step moves to the right, as expected, but stops when its receding contact line gets pinned by the step. Droplets completely located on the left part of the substrate move away from the chemical step, that is, *away* from the *more* wettable substrate, with the velocity decreasing as the distance from the step increases. These numerical results are in complete agreement with our analysis of the effective DJP induced force.

D. Chemical Steps with Coating Layers. $\partial_x \theta(x)$ will be non-monotonous even for $q = 1$ if the long-ranged contributions to the DJP have a different sign for the two sides of the substrate. As an example, Figure 7 shows a contour plot of the disjoining pressure in the vicinity of the chemical step for the $\oplus$ case on the left side and the $\ominus$ case on the right side. In the plus case, the disjoining pressure approaches zero from above as $y \to \infty$, while in the minus case it is negative for all $y > y_0$. Therefore, contour lines corresponding to positive values occur only on the left-hand side. Figure 8 shows $\theta(x)$ and $f(\bar{x})$ for the same values of $B^{(l)}$, $B^{(r)}$, q, and $C^{(l)}$ as in Figure 7 but for various values of $C^{(r)}$. $\partial_x \theta(x)$ is positive outside a narrow region around the chemical step. This indicates that the droplet will move to the left independent of the relative values of $\theta_{eq}^{(l)}$ and $\theta_{eq}^{(r)}$, although it will be pinned at the step if coming from the right. This is confirmed by the analysis of $f(\bar{x})$ in Figure 8b. If both contact lines are on the same side of the step, one has $f(|\bar{x}| > a) < 0$. However, if the droplet spans the step, that is, for $|\bar{x}| < a$, the force is positive for $\theta_{eq}^{(l)} > \theta_{eq}^{(r)}$ (here, for $C^{(r)} < 1$) and negative for $\theta_{eq}^{(l)} < \theta_{eq}^{(r)}$. In this case, the drop is driven toward the more wettable part of the substrate.

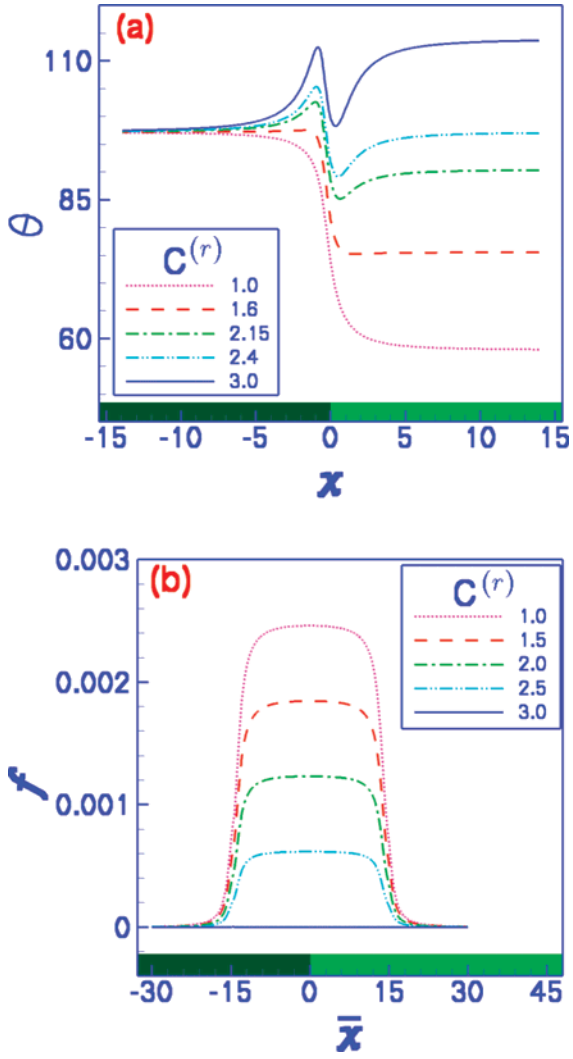

Figure 5. (a) "Local contact angle" $\theta(x)$ (eq 15) and (b) lateral forces $f(\bar{x})$ (eq 16) for droplets with $a = 15$ in the vicinity of a chemical step between two substrates with $C^{(l)} = 3$, $B^{(l)} = B^{(r)} = 0$, and $q = 1.25$ for various values of $C^{(r)}$. Both parts of the substrate correspond to the $\ominus$ case. f is measured in units of σ.

V. Discussion

A. Droplets Spanning the Chemical Step. For droplets spanning the chemical heterogeneity, according to eq 17, the lateral DJP induced force per unit ridge length reduces to

$$f = \cos\theta(a) - \cos\theta(-a) \tag{19}$$

For macroscopic droplets, that is, for $a \to \infty$, one has $\theta(a) = \theta_{eq}^{(r)}$ and $\theta(-a) = \theta_{eq}^{(l)}$ (see eqs 8 and 15), and therefore one recovers the following well-known expression for macroscopic liquid ridges:[3,10]

$$f_{macro} = \cos\theta_{eq}^{(r)} - \cos\theta_{eq}^{(l)} \tag{20}$$

For the first cases considered in section IV (i.e., $B^{(l)} = B^{(r)} = 0$ and $q = 0$, see Figure 3), we have $\theta_{eq}^{(r)} < \theta(a)$ and $\theta_{eq}^{(l)} > \theta(-a)$, which implies that $f > f_{macro}$, that is, the macroscopic models underestimate the driving force on the nanodroplets on the chemical step. This is not always the case, in particular if $\theta(x)$ is non-monotonic as in the other two cases considered above (see Figure 5 for $C^{(r)} > 1.6$ and Figure 8). In these cases, we have $\theta_{eq}^{(r)} > \theta(a)$ and $\theta_{eq}^{(l)} < \theta(-a)$, which implies that $f < f_{macro}$. Therefore, the macroscopic models can both over- or underes-

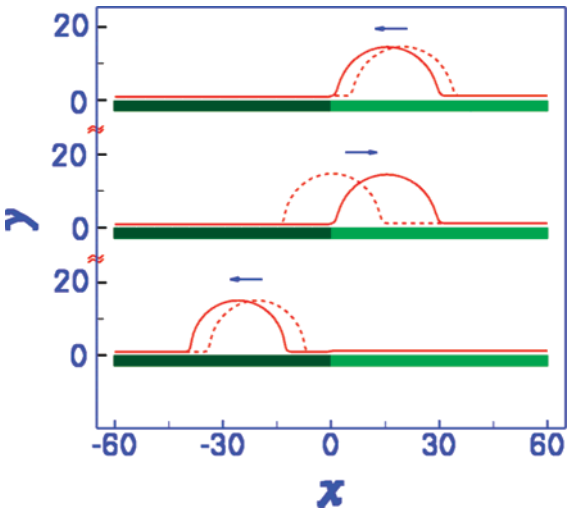

Figure 6. Motion of a nanodroplet near a chemical step in the ⊖ case on both sides, $B^{(l)} = B^{(r)} = 0$, $C^{(l)} = 3$, $C^{(r)} = 2.15$, and $q = 1.25$ (implying $\theta_{eq}^{(l)} = 97.2°$ and $\theta_{eq}^{(r)} = 90.4°$; compare Figure 5), starting at different positions. The droplet shapes are shown, top to bottom, at $t = 170$, 100, and 45 (dashed) and at $t = 4750$, 4300, and 40 000 (solid), respectively.

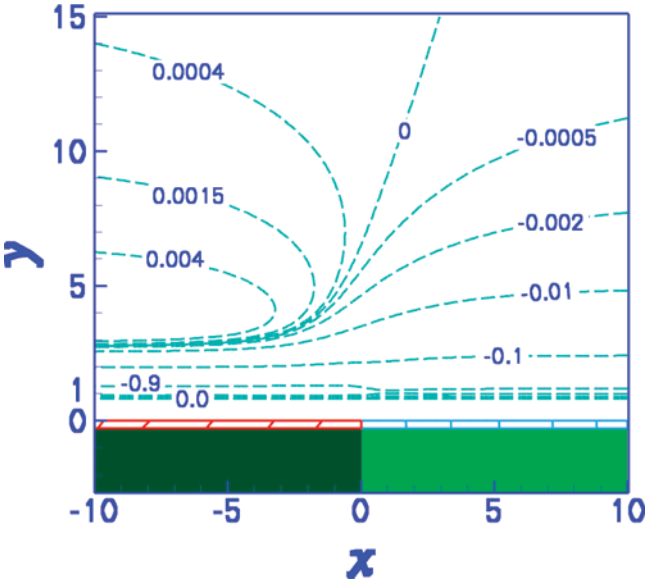

Figure 7. Contour plot of the DJP in the vicinity of a chemical step separating two substrates (⊕ case on the left side, and ⊖ case on the right side) with $B^{(l)} = -2.762$, $C^{(l)} = 2$, $B^{(r)} = -1$, $C^{(r)} = 1$, and $q = 1$ (implying $\theta_{eq}^{(l)} = 73.5°$ and $\theta_{eq}^{(r)} = 77.7°$). The different coatings of the two parts of the substrate associated with the nonzero values of $B^{(l)}$ and $B^{(r)}$ are indicated in the figure.

timate the force on the nanodroplets. However, because $\theta_{eq}(x)$ approaches $\theta_{eq}^{(r)}$ and $\theta_{eq}^{(l)}$ rather rapidly as $x \to \pm\infty$, the differences between the microscopic and the macroscopic force are relatively small.

B. Droplets Completely on one Side of the Step. In contrast to the case in which the droplet spans the step, for droplets which are completely on one or the other side of the step (i.e., with both contact lines on the same side of the step), the force predicted by macroscopic models is exactly zero. Therefore, in this case, even a small force amounts to a qualitative difference in the macroscopic prediction. In all the cases we considered, the direction of motion of a droplet near a chemical step is determined by the sign of $\partial_x \theta(x)$, which is the same as the sign of $-d\Phi(x, y_0(x))/dx$ (see eq 15). Expanding $\Pi(x, y)$ for large $|x|$ up to $O(|x|^{-3})$, one finds on both sides of the step the limiting value for a

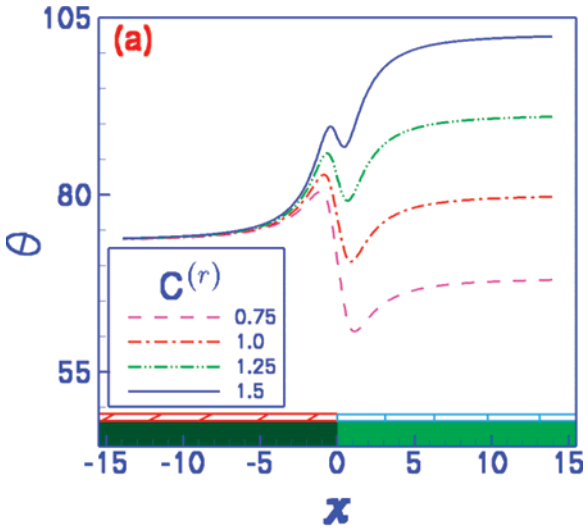

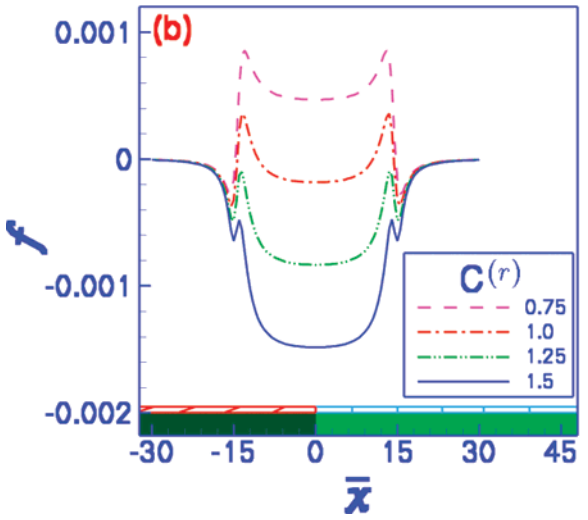

Figure 8. (a) $\theta(x)$ and (b) dimensionless lateral forces $f(\bar{x})$ for droplets with $a = 15$ in the vicinity of a chemical step separating two types of substrates (⊕ case on the left side, and ⊖ case on the right side) with $B^{(l)} = -2.762$, $C^{(l)} = 2$, $B^{(r)} = -1$, $q = 1$, and various values of $C^{(r)}$. f is measured in units of σ. The different coatings of the two parts of the substrate associated with the nonzero values of $B^{(l)}$ and $B^{(r)}$ are indicated in the figures.

homogeneous substrate (see eq 7). This means that the wetting film thickness $y_0(x)$ is independent of x up to this order. To leading order in $1/x$, the sign of $\partial_x \theta(x)$ is therefore given by the partial derivative of $\Phi(x, y_0)$ with respect to x, which happens to be the same on both sides of the chemical step and which is given by

$$\partial_x \theta(x) \simeq \frac{3}{4|x|^3}[-(\pm q^3)C^{(r)} \pm C^{(l)}] + O(|x|^{-4}) \quad (21)$$

with the plus and minus signs in front of $C^{(r)}$ and $C^{(l)}$ corresponding to the ⊕ and ⊖ cases on the right and the left-hand sides, respectively. This means that far from the step the droplets move in the same direction on both sides of the step. For instance, for the case discussed in Figure 5 (with $B^{(l)} = B^{(r)} = 0$), the equilibrium contact angle can be shown to be larger on the right side of the step if $qC^{(r)} > C^{(l)}$, that is, for $C^{(r)} > 2.4$, and the droplets move to the left for $C^{(r)} > C^{(l)}/q^3 = 1.536$ and $|\bar{x}| > a$, in agreement with the numerical results. Equation 21 also indicates that the motion of the droplet is only appreciable near the chemical step.

Our numerical calculations show that for a droplet with $a = 15$ and for the conditions given in Figures 2, 6, and 8 the speed of the droplet reduces drastically for $|w| > 15$.

According to eqs 18 and 21 and the expressions given in section II, it turns out that the lateral force on a droplet in the vicinity of a chemical step is given by the difference of the coefficients of the long-ranged part of the substrate potential only. This allows one to express eq 21 (in its dimensional form) in terms of the Hamaker constants $H^{(l)}$ and $H^{(r)}$ on the left- and right-hand sides, respectively:

$$\partial_x \theta(x) \simeq \frac{3}{4\sigma|x|^3}(H^{(l)} - H^{(r)}) + O(|x|^{-4}) \qquad (22)$$

The dimensional form of eq 18 leads to the following expression for the force on a ridge of width $2a$:

$$f \simeq -\frac{3a \sin\theta(x)}{2|x|^3}(H^{(l)} - H^{(r)}) \qquad (23)$$

We note that in eq 23 the surface tension σ drops out. To this order in $1/x$, the force vanishes if the Hamaker constants on both sides of the chemical step are identical. This is the case if the substrate is chemically structured only by a difference in the surface coating rather than in the bulk substrate itself (see, e.g., ref 34). In this case, the lateral force decays as a function of x according to a power law with an exponent increased by 1, that is, $\sim|x|^{-4}$.

Focusing only at the long-ranged part of the lateral, disjoining pressure induced forces (i.e., for a droplet located completely on one side of the step), the top part of a topographical step (or an edge) as discussed in ref 8 can be considered as an extreme case of a chemical step with one Hamaker constant being exactly zero. For the experimentally frequently used system polystyrene (PS) on silicon, the Hamaker constant is negative with $H_{PS/Si} = -2 \times 10^{-19}$ J.[35,36] Using novel atomic force microscopy based deposition techniques, droplets with diameters less than $2a = 100$ nm can be positioned on a substrate.[37,38] Considering a polystyrene droplet with this diameter positioned at $\bar{x} = 2a$ from a silicon edge, eq 18 predicts a force $f \approx 1.5 \times 10^{-6}$ N/m, which is at least 4 orders of magnitude larger than the gravitational force on a droplet of 100 nm diameter.

However, there are also substrate−liquid combinations with a positive Hamaker constant such as polystyrene on silicon oxide with $H_{PS/SiO} = 2 \times 10^{-20}$ J. For a chemical step formed by two (uncoated) quarter spaces filled by Si and SiO, due to their different sign, the contrast between the two Hamaker constants is higher than that for the edge considered above where one Hamaker constant is zero. Therefore, the lateral force for this compound is larger than the estimate given above for the edge. Since the bulk materials of the step are different, in leading order, the lateral force is independent of a potential coating on either side of the step such as octadecyltrichlorosilane (OTS) or dodecyltrichlorosilane (DTS). Such coatings allow one to change the equilibrium contact angle of polystyrene on Si (with a native SiO layer) from roughly 7° [35,36] (without coating) to about 70° on an OTS or DTS coating.[39] This degree of freedom can be exploited to increase the amplitude of the lateral force (see eq 23) by almost a factor of 10.

C. Experimental Perspectives. Experimentally, a chemical step will be typically accompanied by a small topographical step, for example, on the order of a few angstroms as in ref 34. The aforementioned correspondence between chemical and topographical steps shows that the lateral DJP induced force on a droplet would not be significantly affected by the presence of a change in topography as long as the droplet does not touch the step. These considerations are relevant because typically substrates are chemically patterned by thin coatings rather than by a change in bulk properties. However, with modern lithographic methods, deep trenches with high aspect ratios have been produced, for example, in Si[40] or Ni,[41] which could be filled with another material, realizing chemical steps with changed bulk properties. To observe the phenomena discussed in this paper, the trenches should be at least 100 nm deep (i.e., on the order of the droplet size), but the width can be larger. To obtain larger differences in Hamaker constants, a metallic substrate would be the preferred choice. Preparing smooth surfaces on such substrates to avoid contact line pinning is a challenge, but as a first step it suffices to create smoothness on one side of the chemical step. A further method to produce surfaces with underlying bulk chemical steps is to make cuts through materials containing precipitates or through sintered agglomerates.

In practical terms, a chemical step between Si and SiO bulk materials as considered in the numerical example above is not the best system to verify the theoretical predictions discussed in this paper because under environmental conditions Si is always covered with a native oxide layer of at least a nanometer thickness, which is not thin as compared with the thickness of the wetting layer of polystyrene. This reduces significantly the effective chemical contrast between the two substrate parts. Furthermore, it is not clear whether the deposition methods used in refs 37 and 38 can be applied to polystyrene. The optimal material system to probe the predicted dynamic phenomena would consist of a nonvolatile liquid of which droplets with less than 100 nm diameter can be positioned in the direct vicinity of a step between two materials with Hamaker constants of opposite sign. In addition, the contact angle of the liquid should be rather high at least on one side of the step and pinning should be negligible so that the droplets do not get stuck. Last but not least, the viscosity of the droplets should be moderate such that the droplet motion is neither too fast nor too slow for the experimental observation technique (e.g., optics or electron microscopy). Taking 1 nm and 0.03 N/m as typical values of b and σ, respectively, for the parameters used in Figures 2 and 6, one obtains as the time scale μ/A values of the order of 10^{-8} μ/Pa. For μ between 1000 and 10 000 Pa s (PS at different temperatures[28]), the droplet velocities in our simulations range roughly from 0.1 to 0.01 μm/s. Because the fast initial shape relaxation of the droplet can already lead to significant lateral motion in the vicinity of surface heterogeneities, eventually masking the lateral motion due to the long-ranged dispersion forces, the initial droplet should have a shape close to the relaxed one.

D. The Force on 3D Droplets. Our analysis is restricted to liquid ridges which are translationally invariant along their axes. However, we expect that our arguments and conclusions carry over qualitatively to actual 3D droplets. Equation 16 can be

(34) Checco, A.; Gang, O.; Ocko, B. M. *Phys. Rev. Lett.* **2006**, *96*, 056104.
(35) Seemann, R.; Herminghaus, S.; Jacobs, K. *Phys. Rev. Lett.* **2001**, *86*, 5534.
(36) Seemann, R.; Herminghaus, S.; Jacobs, K. *J. Phys.: Condens. Matter* **2001**, *13*, 4925.
(37) Yang, M.; Sheehan, P. E.; King, W. P.; Whitman, L. J. *J. Am. Chem. Soc.* **2006**, *128*, 6774.
(38) Fang, A.; Dujardin, E.; Ondarçuhu, T. *Nano Lett.* **2006**, *6*, 2368.
(39) Fetzer, R.; Jacobs, K.; Münch, A.; Wagner, B.; Witelski, T. P. *Phys. Rev. Lett.* **2004**, *95*, 127801.
(40) Ansari, K.; van Kan, J. A.; Bettiol, A. A.; Watt, F. *Appl. Phys. Lett.* **2004**, *85*, 476.
(41) Sunami, H.; Matsumura, S.; Yoshikawa, K.; Okuyama, K. *Microelectron. Eng.* **2006**, *83*, 1740.

extended to 3D droplets in a straightforward manner, leading to the following expression for the force F on the droplets:

$$F = \int_{\partial\Omega_d} \Pi(x, y)\, n_x \, dS \tag{24}$$

In contrast to the ridge, the surfaces $\partial\Omega_d$ of 3D droplets are finite.

VI. Summary and Conclusions

In summary, we have outlined a theoretical approach which allows one to study in detail the behavior of nanodroplets near as well as on chemical heterogeneities. Our investigation reveals the dynamics of nanodroplets in the vicinity of chemical heterogeneities caused by long-ranged forces. We have shown that the direction of motion of the droplets is, to leading order in the distance from the step, determined by the competition of the van der Waals forces acting between the droplet and the two different materials of the substrate, that is, the difference in the Hamaker constants (see eq 23), rather than by the equilibrium contact angles which depend also on the short-ranged parts of interaction potentials and on the subleading terms in the disjoining pressure. If the van der Waals forces direct the droplet toward the less wettable material, the droplet will stop as soon as the advancing contact line hits the step. Otherwise, it will continue at a velocity rapidly decreasing with the distance from the step. Droplets which span the chemical step will move toward the more wettable substrate; however, the receding contact line can be pinned by the step.

This study demonstrates that taking into account the effect of long-ranged intermolecular forces is mandatory for accurately controlling and guiding the liquids in open nanofluidic systems. Recent experiments have shown that the arrangement of droplets on structured substrates can be explained by their crossing of chemical steps from the less wettable to the more wettable side.[42] Our study indicates that in general there can be free-energetic barriers to this process which would result in significantly altered patterns. Our analysis also provides a microscopic approach to the pinning and depinning of three-phase contact lines at chemical surface heterogeneities which goes beyond the macroscopic picture of a sharp transition between regions of different wettability on a substrate[23,43−47] or the phenomenological mesoscopic approach of introducing lateral variations of the parameters entering into the effective interface potential.[48]

Acknowledgment. M. R. acknowledges financial support by the Deutsche Forschungsgemeinschaft (DFG) within the priority program SPP 1164 under Grant No. RA 1061/2-1.

Notations and Symbols

a	droplet height, dimensionless
A	material dependent parameter, N/m^2
b	thickness of wetting layer, m
B	coating parameter, dimensionless
C	ratio of intermolecular and surface tension forces (Ab/σ), dimensionless
DJP	disjoining pressure, N/m^2 (in dimensional form)
f	force per unit length, dimensionless
F	force, N
h	film thickness, m
H	Hamaker constant ($\pi^2\Delta N$), J
m	parameter in eq 18
k	Boltzmann constant, 1.38×10^{-23} m^2 kg s^{-2} K^{-1}
M	material parameter, Jm^{12}
n	unit surface normal vector, dimensionless
N	material parameter, Jm^6
p	pressure, dimensionless
r	distance, m
r	distance vector, m
t	time, dimensionless
T	temperature, K
u	velocity vector, dimensionless
x, y, z	coordinates, m (in dimensional form)
$\bar{x}$, $\bar{y}$, $\bar{z}$	droplet center coordinates, dimensionless
y_0	thickness of wetting layer, m (in dimensional form)
w	distance of the nearest edge of the droplet form the step, dimensionless

Greek letters

θ	contact angle
κ	curvature, dimensionless
μ	viscosity, Ns/m^2
Π	disjoining pressure, N/m^2 (in dimensional form)
ρ	number density, m^{-3}
σ	surface tension, N/m
τ	stress tensor
Φ	effective interface potential, J/m^2
ψ	stream function, dimensionless
ω	vorticity, dimensionless
Ω	volume, m^3 (in dimensional form)
$\partial\Omega$	surface, dimensionless

Subscripts

c	coating
d	droplet
eq	equilibrium
g	gyration
l	liquid of the droplet and the wetting layer
l′	surrounding fluid
macro	macroscopic
n	normal
s	substrate
t	tangential
x	lateral
y	vertical
α, β	liquid or solid
$*$	dimensionless

Superscripts

u	upper
$*$	dimensionless
(l)	left-hand side
(r)	right-hand side

(42) Léopoldès, J.; Bucknall, D. G. *Europhys. Lett.* **2005**, *72*, 597.
(43) Casagrande, C.; Fabre, P.; Raphaël, E.; Veyssié, M. *Europhys. Lett.* **1989**, *9*, 251.
(44) Domingues Dos Santos, F.; Ondarçuhu, T. *J. Chim. Phys.* **1996**, *93*, 1991.
(45) Ondarçuhu, T. *J. Phys. II* **1995**, *5*, 227.
(46) Raphaël, E.; de Gennes, P. G. *J. Chem. Phys.* **1989**, *90*, 7577.
(47) Shanahan, M. E. R. *Colloids Surf., A* **1999**, *156*, 71.
(48) Thiele, U. *Phys. Rev. Lett.* **2006**, *97*, 204501.

LA7017677